OPEN ACCESS

University of BRISTOL

Peer reviewed version

Link to published version (if available):
10.1016/j.soildyn.2014.07.008

Link to publication record in Explore Bristol Research

PDF-document

**University of Bristol - Explore Bristol Research**

**General rights**

1-G EXPERIMENTAL INVESTIGATION OF BI-LAYER SOIL RESPONSE AND KINEMATIC PILE BENDING

by

Andrea Chidichimo[1], Roberto Cairo[1], Giovanni Dente[1], Colin A Taylor[2], George Mylonakis[3]


[1] Department of Civil Engineering, University of Calabria, Italy

[2] Department of Civil Engineering, University of Bristol, U.K.

[3] Department of Civil Engineering, University of Patras, Greece

**ABSTRACT**

The effect of soil inhomogeneity and material nonlinearity on kinematic soil-pile interaction and ensuing bending under the passage of vertically propagating seismic shear waves in layered soil, is investigated by means of 1-g shaking table tests and nonlinear numerical simulations. To this end, a suite of scale model tests on a group of five piles embedded in two-layer sand in a laminar container at the shaking table facility in BLADE Laboratory at University of Bristol, are reported. Results from white noise and sine dwell tests were obtained and interpreted by means of one-dimensional lumped parameter models, suitable for inhomogeneous and layered soil profiles, encompassing soil material nonlinearity. A frequency range from 0.1 to 100 Hz and 5 to 35 Hz for white noise and sine dwell tests, respectively, and an input acceleration range from 0.015 to 0.1g, were employed. The paper points out that soil nonlinearity and inhomogeneity strongly affect both site response and kinematic pile bending, so that accurate nonlinear analyses are necessary to predict the dynamic response of pile foundations.

## 1. Introduction

The seismic behavior of pile foundations constitutes a classical problem of soil-structure interaction. Dynamic loads on piles are not only the result of inertial forces induced by the oscillation of the superstructure (*inertial* interaction), but also of deformations of the soil surrounding the pile caused by the propagation of the seismic waves regardless of the presence of a superstructure (*kinematic* interaction).

Studies on dynamic soil-pile interaction have been carried out over the years, mostly by means of numerical approaches such as the finite-element [1-7] and the boundary-element method [8-14].

Among simplified procedures [15], the dynamic Winkler model [16-20] has provided reasonably accurate, versatile and economic alternative to the aforementioned rigorous approaches. Furthermore, the so-called *p-y* curves, originally developed for nonlinear pile-soil interaction under large static or low-frequency cyclic loads, have been extended to the dynamic regime in terms of lumped-parameter formulations encompassing both stiffness and damping using beds of springs and dashpots attached in parallel [21-28]. In recent years, pseudo-static methods, which constitute an essential tool in engineering practice, have been established for the seismic design of piles [29-31]. Similarly, simplified closed-form expressions for the evaluation of kinematic pile bending have been formulated [7,32-36].

On the other hand, experimental studies in the field and the laboratory are more limited, primarily because of cost and complexities in carrying out and interpreting such tests. Following early experiments by Novak and co-workers [37,38], Finn and Gohl [39,40] performed centrifuge tests under earthquake loading on model piles. Shaking table scale model tests on single pile and pile groups were presented by Meymand [41] and large scale shaking table tests on pile-structure models were studied by Tokimatsu et al. [42]. Shirato et al. [43] performed large scale shaking table experiments on a 3x3 pile group, while shaking table tests on a soil-pile-structure model subjected to seismic excitation were performed by Chau et al. [44]. Moccia [45] conducted a large number of shaking table tests on a single pile embedded in layered soil at University of Bristol, in an experimental campaign that preceded the one at hand.

In this paper, small scale model shaking table tests, carried out at the BLADE Laboratory in University of Bristol within the framework of the Seismic Engineering Research Infrastructures for European Synergies (SERIES) project [46,47], are presented and discussed. Tests were performed on both single and grouped piles embedded in a two-layer soil profile. They aimed at assessing the effects of both kinematic and inertial effects, by attaching caps and simple superstructure models on the piles, or testing them under free-head conditions.

The results obtained are interpreted by means of a one-dimensional lumped-parameter model, suitable for heterogeneous and layered profiles, encompassing inertial properties and material nonlinearity. The analyses focus on the nonlinear behavior of the soil and inhomogeneity effects for both site response and kinematic bending of fixed-head piles. Comparisons with simple equations for evaluating kinematic pile bending are also shown.

## 2. Experimental layout and instrumentation

The 1-g shaking table experiments were conducted using a 3 m x 3 m cast aluminium platform weighing 3.8 tonnes, capable of carrying a maximum payload of 15 tonnes. An equivalent shear beam (ESB) container has been used to carry the model soil deposit (Fig. 1). The ESB consists of 8 rectangular aluminium rings, stacked alternately with rubber sections to create a hollow flexible box of inner dimensions 1190 mm long by 550 mm wide and 814 mm deep [48].

## 2.1. Soil profile

Two geo-materials were used to constitute the soil profile: Leighton Buzzard sand fraction B (LBB) and Leighton Buzzard sand fraction E (LBE). Experimental tests are available on these sands to allow a precise characterization [49-51]. The Leighton Buzzard Sand fraction B is constituted by coarse rounded particles with a diameter ranging between 0.6 mm and 1.1 mm. The Leighton Buzzard sand fraction E is a uniform fine sand. Main features of LBE and LBB sands are provided in Table 1. A two-layer soil profile was pluviated into the ESB laminar container (Fig. 2). The free surface of the soil deposit was 800 mm above the laminar container floor. The bottom layer was 460 mm thick, made of LBB and LBE in a 85-15% granular mix, respectively, and for this layer a mass density of 1.78 Mg/m$^3$ had been achieved. The upper layer was 340 mm thick, contained LBE sand, and achieved a mass density of 1.39 Mg/m$^3$.

## 2.2. Model piles arrangement

Five aluminum tubes (commercial model 6063-TS) were used to model the piles (Tab. 2). Each pile was 750 mm long and its head protruded 64 mm above the soil surface. Piles numbering and positioning into the ESB laminar container are depicted in Fig. 2. Piles were aligned in the ESB longitudinal middle plane with two different spacings. Center-to-center distance between piles 1-2 and 2-4 was 140 mm (about 6 pile diameters), whereas for piles 4-5 and 5-3 it was 70 mm (about 3 diameters). Pile 3 was located 455 mm (20 diameters) from the ESB right cross wall while pile 1 was 315 mm (14 diameters) from the ESB left cross wall. During the tests some model configurations were examined under different head constraints [46]. In this work, the following arrangement is discussed: two free-head piles (1 and 2) and a 3x1 pile group (piles 3, 4 and 5) with a restraining cap (Fig. 2).

## 2.3. Dynamic excitations employed

The model was initially subjected to a suite of white noise excitations (Fig. 3) of bandwidth 0.1-100 Hz and input acceleration levels ($a_{base}$) varying from 0.01g to 0.10g. These tests aimed at providing information as to the shear wave propagation velocity and the damping characteristic of the two soil layers.

In a second step, harmonic modulated signals (notably sine dwells) were applied to investigate the dynamic response of the model piles. Sine dwell excitations are composed of 3 linear ramp up cycles, 11 stationary cycles and 3 linear ramp down cycles (Fig. 4). This sequence is important as the input motion needs to be applied to avoid strong transients in the response. Different excitation

frequencies ranging from 5 to 50 Hz were utilized, as well as stationary signal amplitudes between 0.01g and 0.18g.

## 2.4. Monitoring instrumentation

Sixty transducers were employed to instrument the model as summarized in Table 3. Input acceleration at the shaking table was controlled by means of two accelerometers along the x and y direction. Each pile head was equipped with a uniaxial accelerometer in the y direction. Soil response in terms of acceleration was monitored by 7 accelerometers. Five of these instruments were placed along a vertical line in the middle plane of the ESB laminar container (Fig. 5), at a distance from the nearest pile (pile 3) of 85 mm (about 4 pile diameters). The other two were placed out of the middle plane, near the soil surface and the layer interface. Piles 4 and 5 were instrumented with 8 pairs of strain gauges each (Fig. 6), to measure kinematic and inertial-induced curvatures.

In the ESB laminar container (Fig. 1), horizontal displacements were measured by two LVDT's placed on ring 8 (surface level) and ring 5 (layer interface level). Two LVDT's were attached to the heads of piles 4 and 5 for measuring horizontal displacements. A rotation measuring device was installed at the heads of piles 4 and 5. This device is composed by a T-shaped plexiglass plate screwed to the pile head, and two micrometers measuring in the z direction. The difference between the left and right vertical displacements divided by the corresponding distance provides a measure of pile head rotation. An Indikon sensor was installed to measure settlements at soil surface.

## 3.  Soil parameters estimation and materials behavior during the tests

During white noise tests, the accelerations within soil profile (Fig. 5) were filtered and decomposed into harmonics by means of Fourier transforms. In this way, the experimental transfer functions, defined as the ratio of the complex Fourier components of acceleration between any two points of the soil profile, can be obtained.

Figure 8 shows the absolute values (amplification functions) of the upper layer transfer function $F_1(\omega)$ and of $|F(\omega)|$ referred to the entire deposit. These functions have been experimentally obtained through A1, A4 and A6 sensors measures. For a two-layer deposit resting on a rigid base, the theoretical transfer function $F(\omega)$ can be calculated from the familiar expression [54]:

$$F(\omega) = \frac{1}{\cos(\kappa_1 h_1)\cos(\kappa_2 h_2) - \alpha sin(\kappa_1 h_1)\sin(\kappa_2 h_2)} \tag{1}$$

in which ω is the circular excitation frequency; $\kappa_1 = \frac{\omega}{V_{S1}^*}$ and $\kappa_2 = \frac{\omega}{V_{S2}^*}$ are the wave numbers of the upper and lower layer, respectively, $V_{S1}^* = V_{S1}\sqrt{1 + 2i\xi_1}$ and $V_{S2}^* = V_{S2}\sqrt{1 + 2i\xi_2}$ being the complex shear wave velocities of the two layers, having frequency-independent damping ratios $\xi_1$ and $\xi_2$; $h_1$ and $h_2$ are respectively the thickness of the upper and lower layer; $\alpha = \frac{\rho_1 V_{S1}^*}{\rho_2 V_{S2}^*}$ is the impedance ratio of layers, $\rho_1$ and $\rho_2$ being the mass densities of the top and the bottom layer.

Using the above formulation, the shear wave velocities $V_{S1}$ and $V_{S2}$ can be readily determined. Once the experimental frequency response is known, the first mode frequency of the upper layer, $f_N{}^1$, is estimated approximately as the frequency corresponding to the maximum of the amplification function; $V_{S1}$ can then be calculated using the familiar expression $V_{S1} = 4 \cdot f_N{}^1 \cdot h_1$ [32]. The shear wave velocity $V_{S2}$ is estimated based on equation 1 as the value that provides the best fit to the measured data (Fig. 7b). In addition, assuming, as a first-order approximation, the same damping ratio $\xi_S$ for the two layers, this can be determined directly from the amplification function of the whole deposit by the half-power bandwidth method [55].

In Fig. 8 the experimental amplification function versus frequency is reported for different input acceleration levels applied in two sets of white noise tests, which have been indicated with corresponding numbers and codes [46]. Evidently, the natural frequency of the system decreases with amplitude of input motion. Likewise, peak soil amplification decreases with increasing acceleration level at the base. These results suggest that the three frequency response curves displayed in each graph correspond to different strain levels. At greater shear strain amplitudes induced by the shaking motion, a reduction in soil stiffness occurs and the peak of the amplification function moves towards lower frequencies. In addition, internal soil damping increases and maximum soil acceleration attenuates.

For all the performed white noise tests (indicated on the x axis), the back-calculated upper and lower layer shear wave velocity values are shown in Fig. 9, along with the corresponding acceleration levels imposed by the shaking table. This representation allows a visual investigation of dynamic soil response. In particular, for the upper layer (Fig. 9a) three different response stages can be identified: (a) in stage 1, consisting of three consecutive tests, a non-reversible stiffening associated with densification of the loose sand is detected. In fact, as input motion amplitude increases, shear wave velocity increases too; (b) a transient phase (stage 2) in which the upper layer behaves in a linear-like manner, with shear wave velocity amplitude showing little sensitivity in input acceleration amplitude; (c) a residual phase (stage 3), where the upper layer tends to behave as a strain softening material, since shear wave velocity decreases with increasing input motion

amplitude. This tendency is also demonstrated in Fig. 10a, where the three stages are identified. However, for the most part of the excitation campaign, $V_{S1}$ remains almost constant (at approximately 52 m/s). Calculations based on the Hardin and Drnevich [56] and Iwasaki [57] equations provided values in the range 48-65 m/s, which are in meaningful agreement with the back-calculated one.

For the lower soil layer, two different response stages can be identified (Fig. 9b): (a) a non-reversible softening behavior - the opposite to stage 1 shown above - is exhibited early on, corresponding to a decrease in shear wave velocity with increasing acceleration amplitude; (b) the transient and after shaking stages coincide (stage 2) and the granular mix in the specific layer begins to behave as a strain-softening material, since the shear wave velocity decreases with increasing shaking table input motion amplitude. These nonlinear patterns are evident in Fig. 10b.

The variation in damping ratio of the soil deposit, $\xi_S$, for all the data sets examined is plotted in Fig. 11 as a function of base acceleration. Evidently, $\xi_S$ increases or decreases according to the amplitude of base acceleration. A better understanding of the dynamic soil response is provided in Fig. 12. The data shown in white square dots represent the damping ratio of the soil corresponding to the transient phase in which the upper layer behaves as a quasi-linear material (stage 2) and the lower layer stays in the after-shaking stage. The values marked with black square dots refer to the stage 3, in which both layers exhibit a strain-softening behavior. Linear regressions for the two series of data have been made, and are displayed with a dotted line and a continuous line, respectively. These results reveal that when both layers are in the after-shaking stage, i.e. when the entire soil deposit behaves as a strain-softening medium (stage 3), damping increases more rapidly with input acceleration amplitude contrary to the case (stage 2) in which the upper layer behaves as a quasi-linear material and tends to dissipate less energy, since the total hysteresis of the soil system is reduced.

It should be noticed that, for the relatively low strain levels achieved during experiments, damping ratio of the soil has expected to be less than what observed. In general, the half-power bandwidth method, as well as the peak response method, provides values larger than the true ones [55]. However, for the cases examined, this could be explained considering the contribution of the container, as indicated in Fig. 12.

Insight on the nonlinear behavior of the soil deposit can be achieved from the evolution of the free surface settlement measured during tests (Fig. 13), including both white noise and sine dwell experiments. It can be seen that, after the initial phase of soil consolidation in which about 20% of

total settlement occurs (presumably due to the low relative density of the upper layer), a gradual process of densification takes place. Therefore, it is anticipated that the shear modulus of the surface layer increased during the specific phase. The experimental data of the set labelled 101116 have been selected to discuss the analyses presented in the following sections, as they allow assuming a nearly constant value of shear wave velocity $V_{S1}$ of the upper layer, with no increment of the settlement, as highlighted in Fig. 13. A one-dimensional nonlinear lumped-parameter model [58] is employed to interpret the observed soil-pile interaction effects.

## 4. Employed numerical model

In this paper, the dynamic response of a single pile embedded in a two-layer soil excited at the base by vertically propagating shear waves, has been analyzed by means of a lumped-parameter model specifically developed by the authors for the problem at hand (Fig. 14). Driving loads imposed on the pile by the seismic waves propagating in the soil must first be determined by analyzing the free-field response. Both pile and soil are represented by a group of vertically aligned media with lumped masses. Given the low amplitude of the excitation, linear elastic beam elements are used to model the pile. The restraining action of soil is modelled by horizontal springs and dashpots obeying a hyperbolic force-displacement law. The solution is obtained in two consecutive steps: (1) determining the free-field soil motion and (2) predicting the pile response by imposing the free-field soil motion as excitation at the base of the soil springs supporting the pile.

### 4.1 Free-field motion

The equilibrium of the wave-induced horizontal forces in the free-field soil can be expressed in a discrete form as

$$[M]\{\ddot{u}\} + [C]\{\dot{u}\} + [K]\{u\} = \{J\}f(t) \tag{2}$$

where $\{\ddot{u}\}$ is the absolute soil acceleration vector corresponding to the nodes of the model in Fig. 16; $\{\dot{u}\}$ and $\{u\}$ are the corresponding velocity and displacement vectors, respectively; $[M]$ is the lumped-mass matrix, while $[K]$ and $[C]$ are the corresponding stiffness and viscous damping matrices, respectively. Finally, $\{J\}f(t)$ is the load vector applied at the base of the model, $\{J\}$ being a vector with the last term equal to 1 and the rest equal to zero.

The soil must be divided into a suitable number of layers, modeled by a corresponding mass, a nonlinear spring and a viscous dashpot attached in parallel to the spring [59,60]. Mass density $\rho_i$ and shear modulus $G_i$ are constant in each layer of thickness $\Delta z_i$, within a specific time step $\Delta t$.

In this way, the lumped-mass matrix $[M]$ of the system has a diagonal form, and the stiffness matrix $[K]$ is banded. Damping matrix $[C]$, consistent with experimental data, can be determined through the Rayleigh approach [61] depending on mass and stiffness matrices as follows

$$[C] = \alpha_R[M] + \beta_R[K] \tag{3}$$

in which $\alpha_R = 2\xi_S \left( \frac{\omega_N \omega_M}{\omega_N + \omega_M} \right)$ and $\beta_R = 2\xi_S \left( \frac{1}{\omega_N + \omega_M} \right)$ are scalar quantities selected to provide a given damping ratio $\xi_S$ in correspondence of the two control frequencies $\omega_N$ and $\omega_M$ often coinciding with specific modes of vibration. Modes $N$ and $M$ must be selected to ensure reasonable values of $\xi_S$ in each mode contributing significantly to the system dynamic response [62,63]. In this work, the first and third mode were selected, which lead to satisfactory performance of the model over dynamic measurements. Following Joyner and Chen [64], the excitation is expressed as a viscous force, per unit of area, applied at the base of the soil column as

$$f(t) = \rho_R V_S^R \dot{u}_{base}(t) \tag{4}$$

where $\dot{u}_{base}(t)$ is the input velocity time history, $\rho_R$ and $V_S^R$ are mass density and shear wave velocity of the base material, respectively, assumed sufficiently large to model the stiff base under the laminar box. Equation 2 is integrated in the time domain through the β-Newmark scheme [65]. In this study the extended hyperbolic model [66] has been employed to represent the hysteretic behavior of the granular soils. Accordingly, the stress-strain backbone curve is expressed by the equation

$$\tau = \frac{\gamma G_{MAX}}{1 + \beta \left( \frac{\gamma}{\gamma_r} \right)^s} \tag{5}$$

in which $\gamma$ and $\tau$ are the shear strain and stress respectively, $G_{MAX}$ is the initial shear modulus, $\gamma_r$ a reference strain, $\beta$ and $s$ are model parameters, usually estimated with best fitting experimental results. Masing criteria [67] are used for driving the unloading and reloading branches from the skeleton curve. Reference strain $\gamma_r$ is determined following Matasovic and Vucetic [66] as

$$\gamma_r = \frac{\tau_{mo}}{G_{MAX}} \tag{6}$$

$\tau_{mo}$ being the shear stress related to a strain of approximately 1%. It should be noticed that $\gamma_r$ is the yield strain of an elastic-perfectly plastic soil having an elastic shear modulus equal to $G_{MAX}$, depending on the soil shear strength and is implicitly related to confining pressure, $\sigma'$ [60,68]. Values for parameters $\beta$, $\gamma_r$ and $s$ in the two layers are provided in the following.

## 4.2. Pile response

The equation of dynamic equilibrium of the pile component can be written as

$$[M_P]\{\ddot{y}\} + [K_P]\{y\} + \{p\} = 0 \tag{7}$$

where $[M_P]$ and $[K_P]$ are the pile mass and stiffness matrices, respectively; $\{\ddot{y}\}$ is the absolute lateral acceleration vector, $\{y\}$ is the corresponding displacement vector and $\{p\}$ is the soil reaction vector. Since the external loads applied along the pile are in the form of horizontal forces, pile rotations can be eliminated by static condensation [69] to provide $[K_P]$.

For a generic mass constituting the pile, soil reaction can be expressed as

$$p = k_S(y - u) + c_S(\dot{y} - \dot{u}) \tag{8}$$

in which $u$ and $\dot{u}$ are the free-field displacement and velocity, respectively, at given time and depth; $k_S$ is the stiffness of the spring; $c_S$ is the dashpot coefficient. Following Kavvadas and Gazetas [19], these model parameters can be calculated from the expressions

$$k_S = \delta E_S \tag{9}$$

$$c_S = 2\xi_S \frac{k_S}{\omega} \tag{10}$$

$E_S$ being the Young's modulus of soil, $\delta$ a dimensionless soil stiffness parameter, $\xi_S$ the soil damping ratio and $\omega$ the frequency of input motion. Typical values of $\delta$ vary between 0.8 and 1.5 [17,23,70,71]. Kavvadas and Gazetas [19] showed that, contrary to pile displacements, bending moments can be sensitive to spring stiffness, which may attain values up to $4E_S$ in heterogeneous soil. In the present study the fitted formula proposed by Syngros [72] is employed

$$\delta = 2\left(\frac{E_P}{E_S}\right)^{-0.075} \tag{11}$$

$E_P$ being the Young's modulus of the pile.

## 5. Theoretical results versus experimental evidences

### 5.1. Soil model parameters

The 1-D lumped parameter model used in the simulations at hand is shown in Fig. 14. The experimental data under consideration refer to the 12 sine dwell input signals applied during 101116 experimental set. These harmonic excitations have frequencies $f$ varying between 5 to 35 Hz and amplitudes $a_{base}$ ranging between 0.0155g to 0.0452g (Table 4). Two different shear wave velocity profiles are considered (Fig. 15): for profile A, $V_{S1}$=52 m/s and $V_{S2}$=87 m/s for the upper and lower layer, respectively, are assumed as low strain (initial) values. In profile B a constant value of $V_{S2}$=80 m/s is adopted, whereas $V_{S1}$ is considered to vary with depth according to the parabolic law [73]

$$V_{S1}(z) = V_{h1}\left[b + (1 - b)\frac{z}{h_1}\right]^n \tag{12}$$

In this equation, $V_{h1}$ is the shear wave velocity value at the layer interface, $h_1$ is the upper layer thickness, $b = \left(\frac{V_0}{V_{h1}}\right)^{\frac{1}{n}}$ is an inhomogeneity coefficient, and $n$ is a rate of inhomogeneity parameter (usually varying between 0.2 and 0.3 for sands), $V_0$ is the shear wave velocity at the soil surface. The following parameters are used in the realm of profile B: $V_{h1}$=60 m/s, $V_0$=40 m/s, $n$ =0.25.

All the above parameters are introduced to define the initial material properties of the soils. They have been selected as the quantities, for the soil profiles considered, that allow a better curve-fitting of the experimental amplitude function (Fig. 16) corresponding to the lowest amplitude white noise test considered.

The parameters required to define the hyperbolic backbone curve implemented in the present approach are estimated as follows: linear regressions have been applied on the experimental V<sub>S</sub>=*f*(a<sub>base</sub>) dependence obtained from the white noise tests performed immediately before and after the suite analysed (Table 4), for both the upper and bottom layers (Fig.17a). Similarly, a linear regression is carried out on the ξ<sub>S</sub>=*f*(a<sub>base</sub>) dependence (Fig. 17b). This allows determining the variation of shear wave propagation velocity and damping ratio with input acceleration level in the two soil layers.

The shear modulus reduction curves, $G_{S1}(\gamma)$ and $G_{S2}(\gamma)$, of the soil layers (Fig. 18a) are back-calculated by means of the following linear equivalent technique, applied to soil profile A: in correspondence of the natural frequency of the soil deposit, elastic analyses are performed for different input acceleration levels, $a_{base}$, fixing the model mechanical parameters ($V_{S1}, V_{S2}$ and $\xi_S$)

11

in accordance to the aforementioned functions, $V_S(a_{base})$ and $\xi_S(a_{base})$. In these analyses, the maximum shear strains, γ, are calculated at the middle points of the upper and lower layer. In this way, the ratios $G/G_{MAX}(\gamma)$ indicated with symbols in Fig. 18a are determined. These extrapolated points are then fitted by means of Equation 5 to be used in the nonlinear simulations. For comparison, the reduction curve by Vucetic and Dobry [74] corresponding to a null plastic index is also shown. In addition, Figure 18b shows the hysteretic damping provided by the hyperbolic model adopted. For the strain level attained, the values obtained can be considered reasonable.

## 5.2. Free-field response

A comparison between the theoretical and experimental acceleration profiles along the soil deposit for 6 sine dwell input excitations with different frequencies ($f$) and amplitudes ($a_{base}$) is shown in Fig. 19. The modulus of maximum acceleration achieved with depth $z$ is shown in terms of the dimensionless ratio $a_{max}/a_{base}$. The experimental data are depicted with dots, the calculated accelerations for soil profile A are indicated with a dotted line, whereas those for soil profile B are reported with a full line. These results have been obtained considering linearly elastic soil behavior. It can be noticed that these solutions do not agree well with the measured values. A similar comparison, where the free-field soil response has been calculated with nonlinear analyses is shown in Fig. 20. As can be seen, the comparison is much more satisfactory, especially for soil profile B.

For each of the sine dwell excitations considered, the ratio of the recorded maximum acceleration amplitude at the free surface to the input base acceleration is plotted in Fig. 21, marked with black dots. The theoretical amplification functions are also shown. They have been calculated for both soil profiles A and B, with both linear and nonlinear response analyses.

As can be noticed, the experimentally observed frequency response is well reproduced only when nonlinearity is considered. Moreover profile B matches better the experimental results.

In addition, stress-strain loops obtained by means of the lumped-parameter model, for both the upper and lower layer middle points are displayed in Fig. 22, for the 25 Hz sine dwell type input. It is observed that, for the applied acceleration level, the top layer of sand behaves essentially as an elastic material with very low hysteresis. On the contrary, for the bottom layer granular mix, a shear modulus decay and a hysteretic damping are obtained. These results are in agreement with the observed experimental evidence, demonstrating that nonlinearity is mainly associated with the bottom layer in the cases examined.

## 5.3. Pile kinematic bending

In this section bending strains along piles 4 and 5 are shown. Theoretical results are also presented for profile B. Elastic solutions (dotted line) and nonlinear analyses (full line) are compared against measurements for pile 4 (black dots) and 5 (white squares) in Fig. 23. In the same vein as before, the results obtained by nonlinear analysis are in good agreement with measured value. Major differences can be noticed at the proximity of the pile head. These differences should be expected, since the fixing device at the pile head cannot be considered as a perfect no-rotational fixity. In fact, a rotational compliance at the pile head can justify the lower bending strain measured in that location.

Figure 24 presents the bending strains within the frequency range of the tests at hand and highlights the strong influence of soil nonlinearity on kinematic pile bending. As can be seen, soil nonlinearity results in a strong attenuation of kinematic bending at the interface between the soil layers. These results are well reproduced by the analysis.

Moreover, it is possible to observe that de-resonance of the soil deposit causes a reduction and a shift toward lower frequencies of the maximum bending strain developing at the pile heads. This is in accordance with available evidence [75-77] that pile head kinematic bending is strongly related to the maximum acceleration at the free surface.

For the sake of completeness, kinematic bending strains at the layer interface calculated with the proposed approach are compared to those obtained with few closed-form expressions available in the literature (Fig. 25).

Adopting a simplified Winkler model, Mylonakis [32] defined a strain transmissibility parameter as the ratio between peak pile bending strain and free-field soil shear strain at the interface, $\gamma_1$, which is a function of the layer stiffness contrast, the embedment ratio of the pile in the upper layer and the soil-pile stiffness contrast associated with the surface layer. The author suggested to take into account the effect of the frequency by means of a correction function $\Phi$. In this work the dynamic factor $\Phi_2$ proposed by Sica et al. [36] has been employed.

To overcome some limitations of the Mylonakis [32] approach, Di Laora et al. [7] developed a simple regression formula for the strain transmissibility parameter, capable of accounting for the dependence of ground response on frequency.

Nikolaou et al. [33] obtained an empirical equation for the pile kinematic moment at the interface in resonant steady-state conditions. Besides pile slenderness, pile-soil stiffness and shear wave velocity contrast, this relation is based on the shear stress at the interface induced in the free-field by seismic motion. Maiorano et al. [34] revised this expression introducing a dynamic coefficient $\beta$ depending on the occurrence of resonance, and the transient peak soil shear strain $\gamma_1$ at the interface.

13

As can be observed from Fig. 25, the selected formulae compare well with the present approach, both under the assumption of linear and nonlinear behavior of the soil deposit. The maximum shear strain $\gamma_1$ has been determined, for each frequency, through a site response analysis carried out with the lumped-parameter model at hand. In the case of nonlinear analyses, the calculated values of shear strains of the two layers have been used to evaluate the proper shear moduli from the reduction curves adopted.

## 6 Concluding remarks

Soil-pile kinematic bending was investigated by means of shaking table tests. Results have been interpreted by means of Fourier transforms and comparisons against a simplified 1-D approach involving the pile and the soil as interconnected columns. Results proved that soil nonlinearity and inhomogeneity can strongly affect both free-field and kinematic pile response. From the interpretation of the experimental evidence, the following conclusions can be drawn:

1. Soil nonlinearity drastically affects the free-field motion. Increasing the input motion amplitude leads to a decrease in resonant frequency and an increase in soil damping ratio. For the cases examined, this behavior can be mainly attributed to the response of the bottom soil layer.
2. Soil inhomogeneity is an important factor in controlling free-field response.
3. Experimental results have been satisfactorily reproduced by means of the nonlinear numerical analyses reported in the article. Geometric and material properties are adequately represented by the hyperbolic stress-strain relations to simulate the nonlinear behavior of sand.
4. Whereas elastic solutions are useful for understanding the fundamentals of kinematic interaction, they can lead to wrong estimation of kinematic bending both at the layer interfaces and the pile head. More precise analyses require that the nonlinear behavior of the soil should be taken into account.
5. Experimental evidence demonstrated a strong correlation between soil surface acceleration and kinematic bending at the pile head. As a result, elastic solutions are not expected to predict satisfactorily the frequency at which maximum bending strain develops at the pile head.

## List of Symbols

| | |
|---|---|
| $a_{base}$ | input acceleration level |
| $b$ | inhomogeneity coefficient |
| $[C]$ | damping matrix of soil column |
| $c_S$ | soil-pile interface dashpot coefficient |
| $C_u$ | uniformity coefficient |
| $D_{10}, D_{50}, D_{60}$ | grain size diameters |
| $E_P$ | Young's modulus of the pile |
| $E_S$ | Young's modulus of soil |
| $f$ | frequency |
| $f_N{}^1$ | first mode frequency of the top layer |
| $f(t)$ | Viscous force applied at the base of the soil column |
| $F(\omega)$ | transfer function of the soil deposit |
| $F_1(\omega)$ | transfer function of the top layer |
| $G_{MAX}$ | elastic soil shear modulus |
| $G_{S1}, G_{S2}$ | shear modulus in top and bottom soil layers, respectively |
| $h_1, h_2$ | thickness of top and bottom soil layers, respectively |
| $[K]$ | stiffness matrix of soil column |
| $[K_P]$ | stiffness matrix of the pile |
| $k_S$ | Winkler spring coefficient |
| $[M]$ | masses matrix of soil column |

| | |
|---|---|
| $[M_P]$ | masses matrix of the pile |
| $n$ | rate of inhomogeneity parameter |
| $t$ | time |
| $u$ | free-field soil displacement |
| $V_0$ | Shear wave velocity in the top layer (value at the soil surface) |
| $V_{h1}$ | Shear wave velocity in the top layer (value at the layer interface) |
| $V_{S1}, V_{S2}$ | shear wave velocities in top and bottom soil layers, respectively |
| $V_{S1}{}^*, V_{S2}{}^*$ | complex shear wave velocities in top and bottom soil layers, respectively |
| $V_S^R$ | shear wave velocity in the bedrock |
| $y$ | Pile displacement |
| $z$ | Vertical coordinate |
| $\alpha$ | impedance ratio of soil layers |
| $\alpha_R, \beta_R$ | Rayileigh coefficents |
| $\gamma$ | soil shear strain |
| $\gamma_r, \beta, s$ | hyperbolic model parameters |
| $\delta$ | Dimensionless parameter relating $k_s$ and $E_s$ |
| $\kappa_1, \kappa_2$ | complex wave numbers in top and bottom soil layers, respectively |
| $\xi_S, \xi_1, \xi_2$ | damping coefficients of soil material |
| $\rho_1, \rho_2$ | mass densities in top and bottom soil layers, respectively |
| $\rho_R$ | mass density in the bedrock |
| $\sigma'$ | Confining pressure |
| $\tau$ | soil shear stress |
| $\tau_{mo}$ | Shear stress related to a strain of approximately 1%. |
| $\omega$ | Cyclic oscillation frequency |
| $\omega_N, \omega_M$ | Rayleigh damping control frequencies |

## 7   References

[1] Angelides DC, Roesset JM. Nonlinear lateral dynamic stiffness of piles. J. Geotech. Eng. Div. ASCE 1981; 107(GT11):1443-1460.

[2] Wu G, Finn W. Dynamic elastic analysis of pile foundations using finite element method in the time domain. Can. Geotech. Journal 1997; 34:44-52.

[3] Cai YX, Gould PL, Desai CS. Nonlinear analysis of 3D seismic interaction of soil–pile–structure system and application. Engineering Structures 2000; 22(2):191–199.

[4] Kimura M, Zhang F. Seismic evaluation of pile foundations with three different methods based on three-dimensional elasto-plastic finite element analysis. Soils and Foundation 2000; 40(5):113-132.

[5] Maheshwari BK, Truman KZ, El Naggar MH, Gould PL. Three-dimensional finite element nonlinear dynamic analysis of pile groups for lateral transient and seismic excitations. Canadian Geotechnical Journal 2004; 41:118-133.

[6] Dezi F, Carbonari S, Leoni G. A model for the 3D kinematic interaction analysis of pile groups in layered soils. Earthquake Engineering and Structural Dynamics 2009; 38(11):1281-1305.

[7] Di Laora R, Mandolini A, Mylonakis G. Insight on kinematic bending of flexible piles in layered soil. Soil Dynamics and Earthquake Engineering 2012; 43:309-322.

[8] Kaynia AM, Kausel E. Dynamic stiffness and seismic response of pile groups. Research Report R82-03 1982; Massachusetts Institute of Technology.

[9] Kaynia A, Kausel E. Dynamics of piles and pile groups in layered soil media. Soil Dynamics and Earthquake Engineering 1992; 10:386–401.

[10] Mamoon SM, Banerjee PK. Response of piles and pile groups to travelling SH-waves. Earthquake Engineering and Structural Dynamics 1990; 19(4):597-610.

[11] Kaynia AM, Novak M. Response of pile foundations to Rayleigh waves and obliquely incident body waves. Earthquake Engineering and Structural Dynamics 1992; 21(4):303-318.

[12] Kaynia AM, Mahzooni S. Forces in pile foundations under seismic loading. Journal Engineering Mechanics ASCE 1996; 122:46-53.

[13] Guin J, Banerjee PK. Coupled soil-pile-structure interaction analysis under seismic excitation. Journal of Structural Engineering ASCE 1998; 124(4):434-444.

[14] Cairo R, Dente G. Kinematic interaction analysis of piles in layered soils. In: Geotechnical Aspects of EC8, XIV European Conference on Soil Mechanics and Geotechnical Engineering 2007; Paper no. 13, (cd-rom).

[15] Pender MJ. Aseismic pile foundation design analysis. Bulletin of the New Zealand National Society for Earthquake Engineering 1993; 26(1): 49-160.

[16] Novak M, Aboul-Ella F. Stiffness and damping of piles in layered media. In: ASCE Specialty Conf. on Earthquake Engineering and Soil Dynamics 2 1978; p. 704-719.

[17] Dobry R, Vincente E, O'Rourke MJ, Roesset JM. Horizontal stiffness and damping of single piles. Journal of Geotechnical Engineering Div. ASCE 1982; 108(3):439-459.

[18] Nogami T. Flexural responses of grouped piles under dynamic loading. Earthquake Engineering and Structural Dynamics 1985; 13(3):321-336.

[19] Kavvadas M, Gazetas G. Kinematic response and bending of free-head piles in layered piles. Geotechnique 1993; 43(2):207-222.

[20] Mylonakis G, Nikolaou A, Gazetas G. Soil-pile-bridge seismic interaction: kinematic and inertial effects. Part 1: soft soil. Earthquake Engineering and Structural Dynamics 1997; 26:337-359.

[21] Penzien J. Soil-pile foundation interaction. In: Wiegel RL, editor. Earthquake Engineering, 1970; p. 349-381.

[22] Matlock H, Foo SHC, Bryant LM. Simulation of lateral pile behavior under earthquake motion. In: Specialty Conf. on Earthquake Engineering and Soil Dynamics 1978; p. 600-619.

[23] Kagawa T, Kraft LM. Lateral pile response during earthquakes. J. Geotechnical Engineering Div. ASCE 1981; 107(12):1713-1731.

[24] Nogami T, Otani J, Chen HL. Nonlinear soil-pile interaction model for dynamic lateral motion. Journal of Geotechnical Engineering ASCE 1992; 118: 89-106.

[25] El Naggar MH, Novak M. Nonlinear analysis for dynamic lateral pile response. Soil Dynamics and Earthquake Engineering 1996; 15:233-244.

[26] Boulanger RW, Curras CJ, Kutter BL, Wilson DW, Abghari A. Seismic soil-pile-structure interaction experiments and analyses. Journal of Geotechnical and Geoenvironmental Engineering ASCE 1999; 125(9):750-759.

[27] Gerolymos N, Gazetas G. Phenomenological model applied to inelastic response of soil-pile interaction system. Soils and Foundations 2005; 45(4):119-132.

[28] Cairo R, Conte E, Dente G. Nonlinear seismic response of single piles. In: 2008 Seismic Engineering Conference commemorating the 1908 Messina and Reggio Calabria Earthquake (MERCEA) Vol. 1 2008; p. 602-609.

[29] Tabesh A, Poulos HG. Pseudostatic approach for seismic analysis of single piles. Journal of Geotechnical and Geoenvironmental Engineering ASCE 2001; 127(9):757-765.

[30] Castelli F, Maugeri M. Simplified approach for the seismic response of a pile foundation. Journal of Geotechnical and Geoenvironmental Engineering ASCE 2009; 135(10):1440-1451.

[31] Dezi F, Carbonari S, Leoni G. Static equivalent method for the kinematic interaction analysis of single piles. Soil Dynamics and Earthquake Engineering 2010; 30:679-690.

[32] Mylonakis G. Simplified method for seismic pile bending at soil layer interfaces. Soils and Foundations 2001; 41(4):47-58

[33] Nikolaou S, Mylonakis GE, Gazetas G, Tazoh T. Kinematic pile bending during earthquakes: analysis and fields measurements. Géotechnique 2001; 51(5):425-440.

[34] Maiorano RMS, de Sanctis L, Aversa S, Mandolini A. Kinematic response analysis of piled foundations under seismic excitation. Canadian Geotechnical Journal 2009; 46:571-584.

[35] Dezi F, Carbonari S, Leoni G. Kinematic bending moments in pile foundations. Soil Dynamics and Earthquake Engineering 2010; 30:119-132.

[36] Sica S, Mylonakis G, Simonelli AL. Transient kinematic pile bending in two-layer soil. Soil Dynamics and Earthquake Engineering 2011; 31:891-905.

[37] Novak M, Grigg RF. Dynamic experiments with small pile foundations. Canadian Geotechnical Journal 1976; 13:372-385.

[38] El Sharnouby B, Novak M. Dynamic experiments with group of piles. Journal of Geotechnical Engineering Div. ASCE 1984; 110(6):719-737.

[39] Finn WDL, Gohl WB. Centrifuge model studies of piles under simulated earthquake lateral loading. In: Nogami T, editor. Dynamic response of pile foundations – Experiment, analysis and observation. Geotechnical Special Publication No. 11. ASCE 1987; p. 21-38.

[40] Finn WDL, Gohl WB. Response of model pile groups to strong shaking. In: Prakash S, editor. Piles under dynamic loads. Geotechnical Special Publication No. 34. ASCE 1992; p. 27-55.

[41] Meymand PJ. Shaking table scale model tests of nonlinear soil-pile-superstructure interaction in soft clay. PhD dissertation, University of California, Berkley 1998.

[42] Tokimatsu K, Suzuki H, Sato M. Effects of inertial and kinematic interaction on seismic behavior of pile with embedded foundation. Soil Dynamics and Earthquake Engineering 2005; 25:753-762.

[43] Shirato M, Nonomura Y, Fukui J, Nakatani S. Large-scale shake table experiment and numerical simulation on the nonlinear behavior of pile-groups subjected to large-scale earthquake. Soils and Foundations 2008; 48(3):375-396.

[44] Chau KT, Shen CY, Guo X. Nonlinear seismic soil-pile-structure interactions: Shaking table tests and FEM analyses. Soil Dynamics and Earthquake Engineering 2009; 29:300-310.

[45] Moccia F. Seismic soil pile interaction: experimental evidence. PhD dissertation, University of Naples 2009.

[46] Chidichimo A. Experimental and analytical investigation on soil-pile-structure interaction. PhD dissertation, University of Reggio Calabria 2014.

[47] Simonelli AL, Di Sarno L, Durante MG, Sica S, Bhattacharya S, Dietz M, Dihoru L, Taylor CA, Cairo R, Chidichimo A, Dente G, Modaressi A, Todo Bom LA, Kaynia AM, Anoyatis G, Mylonakis G. Experimental assessment of seismic pile-soil interaction. In: Ilki A. and Fardis MN,

editors. Seismic Evaluation and Rehabilitation of Structures. Geotechnical, Geological and Earthquake Engineering Vol. 26, Ch. 26, 2014; p. 455-475.

[48] Crewe AJ, Lings ML, Taylor CA, Yeung AK, Andrighetto R. Development of a large flexible shear stack for testing dry sand and simple direct foundations on a shaking table. In: Elnashai AS, editor. European Seismic Design Practice 1995.

[49] Çabalar AF. Effects on fines content on the behavior of mixed samples of a sand. Electronical Journal of Geotechnical Engineering 2008; 13(D).

[50] Cavallaro A, Maugeri M, Mazzarella R. Static and dynamic properties of Leighton Buzzard sand from laboratory tests. In: 4th International Conference on Recent Advances in Geotechnical Earthquake Engineering and Soil Dynamics 2011.

[51] Sica S, Mylonakis G, Simonelli AL. Strains effect on kinematic bending in layered soils. Soil Dynamics and Earthquake Engineering 2013; 49:231-242.

[52] Cai Y. An experimental study of non-coaxial soil behavior using hollow cylinder testing. PhD dissertation, University of Nottingham 2010.

[53] Visone C. Perfomance-based approach in seismic design of embedded retaining walls. PhD dissertation, University of Naples 2008.

[54] Cairo R, Dente G, Sica S, Simonelli AL. Multi-variable relations for simplified evaluation of soil-pile kinematic effects. Italian Geotechnical Journal 2011; 11(1):33-46.

[55] Seybert AF. Estimation of damping from response spectra. Journal of Sound and Vibration 1981; 75(2):199-206.

[56] Hardin BO, Drnevich VP. Shear modulus and damping in soils: measurement and parameter effects. Journal of the Soil Mechanics and Foundations Divisions ASCE 1972; 98(6):603-624.

[57] Iwasaki T, Tatsuoka F, Takagi Y. Shear modulus of sands under torsional shear loading. Soils and Foundations 1978; 18(1):29-56.

[58] Cairo R, Chidichimo A. Nonlinear analysis for pile kinematic response. In: 5th International Conference on Earthquake Geotechnical Engineering 2011; Paper no. NAFCA.

[59] Kramer SL. Geotechnical Earthquake Engineering. Prentice-Hall 1996.

[60] Phillips C, Hashash YMA. Damping formulation for nonlinear 1D site response analysis. Soil Dynamics and Earthquake Engineering 2009; 29:1143-1158.

[61] Rayleigh JWS, Lindsay RB. The theory of sound. Vol. 2(1), Dover Publications 1945.

[62] Lanzo G, Pagliaroli A, D'Elia B, Influenza della modellazione di Rayleigh dello smorzamento viscoso nelle analisi di risposta sismica locale. In: XI Conference "L'ingegneria Sismica in Italia" 2004 (in Italian).

[63] Park D, Hashash YMA. Soil damping formulation in nonlinear time domain site response analysis. Journal of Earthquake Engineering 2004; 8(2):249–74.

[64] Joyner WB, Chen ATF. Calculation of nonlinear ground response in earthquakes. Bull. Seism. Soc. Am. 1975; 65(5):1315–1336.

[65] Newmark NM. A method of computation for structural dynamics. Journal of the Engineering Mechanics Div. ASCE 1959; 85:67–94.

[66] Matasovic N, Vucetic M. Cyclic characterization of liquefiable sands. Journal of Geotechnical and Geoenvironmental Engineering ASCE 1993; 119(11):1805-1822.

[67] Masing G. Eignespannungen und verfestigung beim messing. In: 2$^{nd}$ International Congress on Applied Mechanics, Zurich, Switzerland 1926; p. 332–335.

[68] Ishihara K. Soil Behaviour in Earthquake Geotechnics. Oxford University Press 1996.

[69] Clough RW, Penzien J. Dynamics of Structures (3$^{rd}$ edition). Computer and Structures, Berkley 2003.

[70] Yoshida I, Yoshinaka R. A method of estimate modulus of horizontal subgrade reaction for a pile. Soils and Foundations 1972; 12(3):1-7.

[71] Roesset JM, Angelides D. Dynamic stiffness of piles. Numerical methods in offshore piling. London: Institution of Civil Engineers 1980; p. 75-81.

[72] Syngros C. Non-linear seismic response of pile-supported structure evaluated trough case histories. PhD dissertation, CUNY 2004.

[73] Rovithis EN, Parashakis H, Mylonakis GE. 1D harmonic response of layered inhomogeneous soil: Analytical investigation. Soil Dynamics and Earthquake Engineering 2011; 31(7):879-890.

[74] Vucetic M, Dobry R. Effect of soil plasticity on cyclic response. Journal of Geotechnical Engineering ASCE 1991; 117(GT1):89-107.

[75] Mylonakis G, Nikolaou A. Design methods for earthquake-induced pile bending. In: Year 2002 International Conference and Exposition. Deep Foundation Institute: Nice 2002.

[76] de Sanctis L, Maiorano RMS, Aversa S. A method for assessing bending moments at the pile head. Earthquake Engineering and Structural Dynamics 2010; 39(10):1133–1154.

[77] Di Laora R, Mylonakis G, Mandolini A. Pile-head kinematic bending in layered soil. Earthquake Engineering and Structural Dynamics 2013; 42(3):319-337.
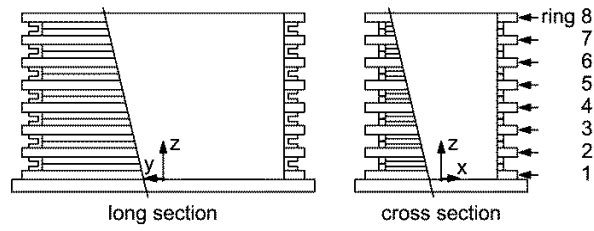
Fig. 1. ESB: Equivalent shear beam laminar container
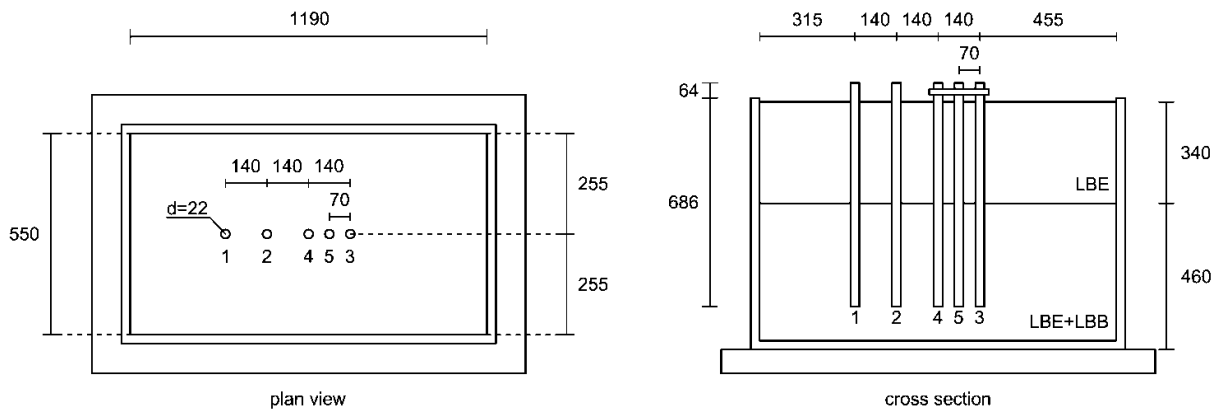


Fig. 2. Soil profile and pile configuration in ESB laminar container (all dimensions in millimeters)
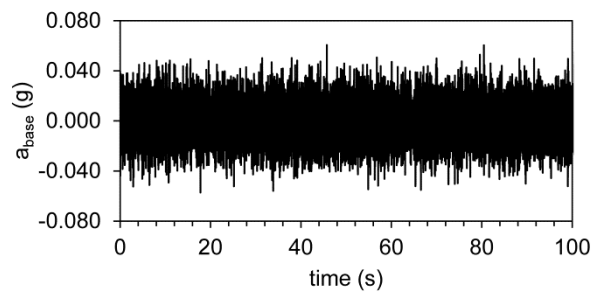


Fig. 3. White noise type signal.
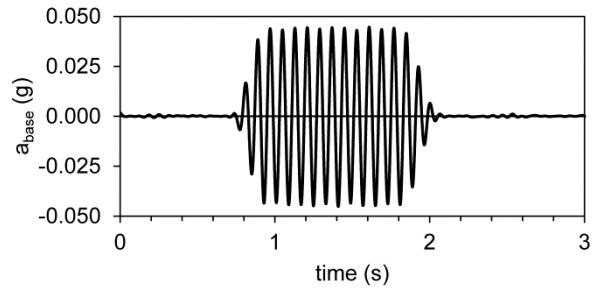
Fig. 4. Sine dwell type signal.
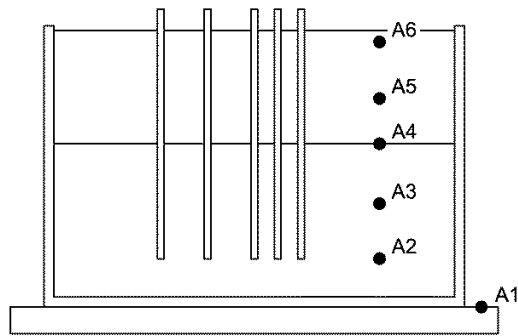


Fig. 5. Vertical accelerometer array in free-field.
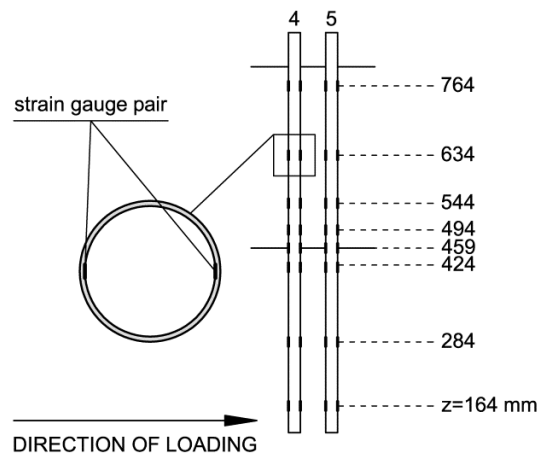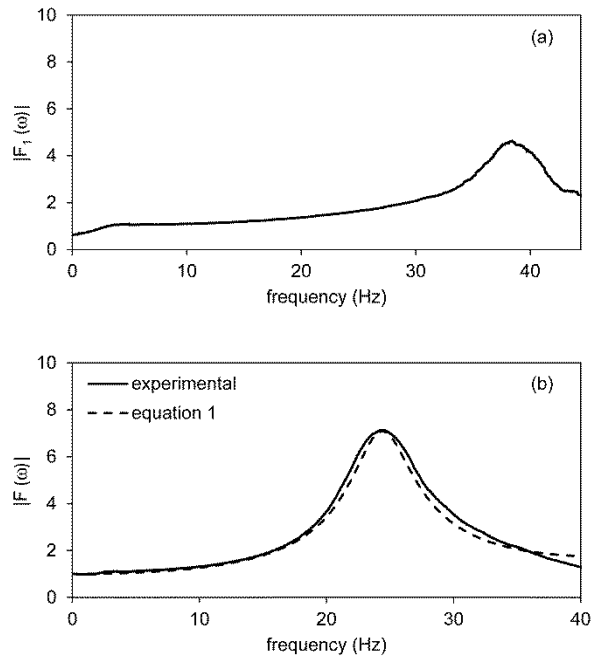


Fig. 6. Strain gauges positioning on instrumented piles.

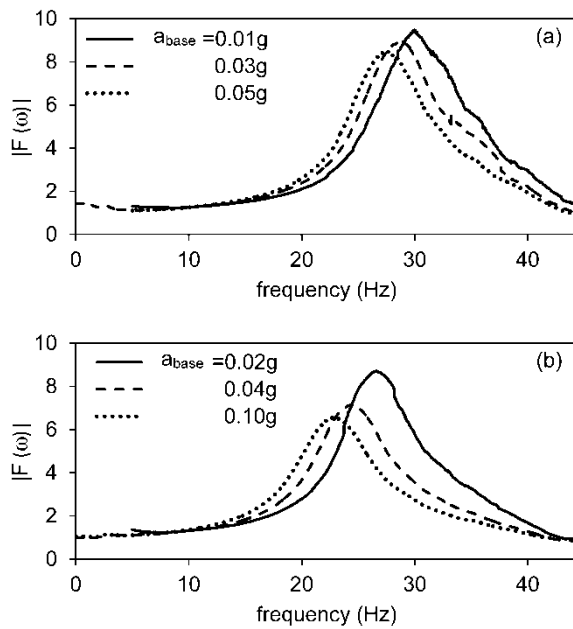Fig.7. Amplification function for the upper layer (a) and the whole deposit (b) for white noise excitation (test 101116_X2); $a_{base}$=0.04g.



Fig.8. Influence of input motion acceleration level on deposit amplification functions for: test set 101115 (a), tests set 101116 (b).
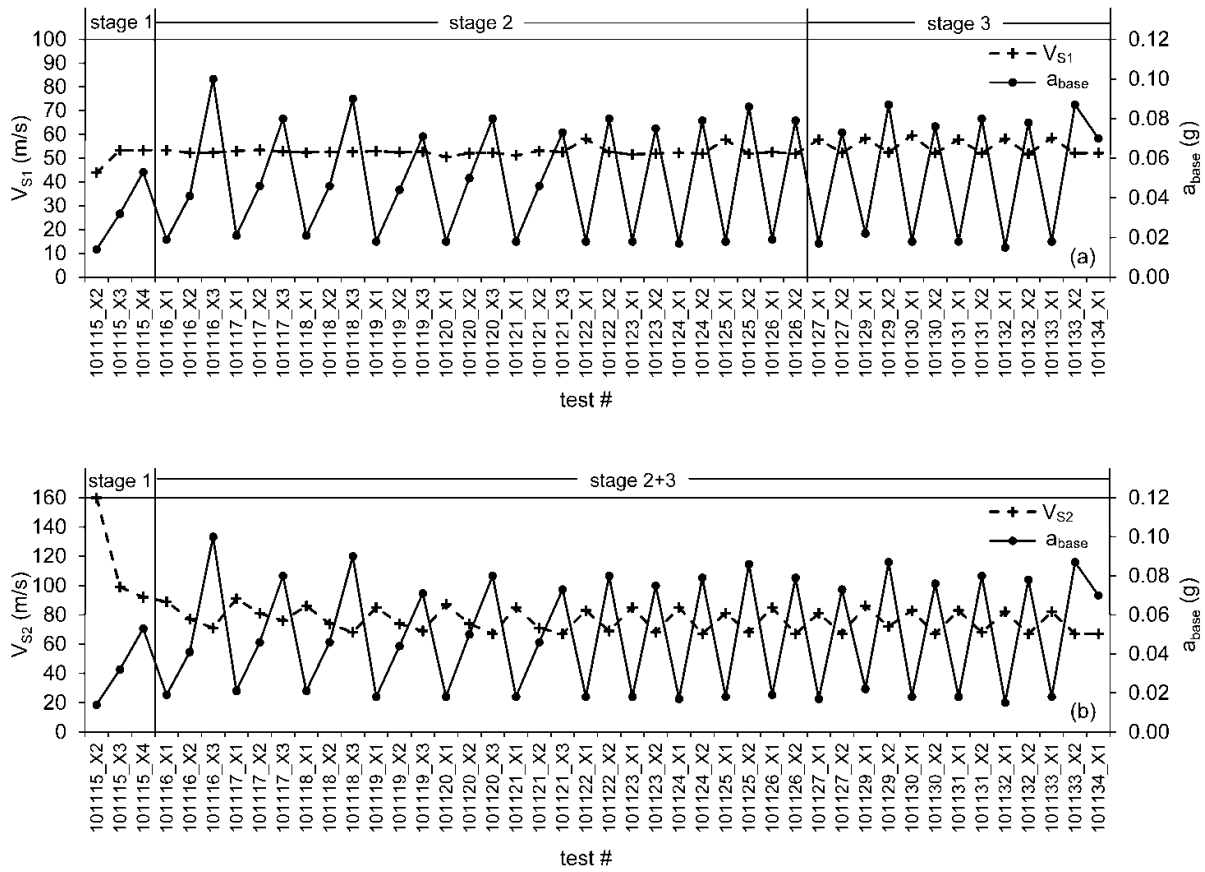
Fig. 9. Back-calculated fit shear wave velocities at top layer (a) and bottom layer (b) during white noise tests. Input acceleration level is shown on the right.
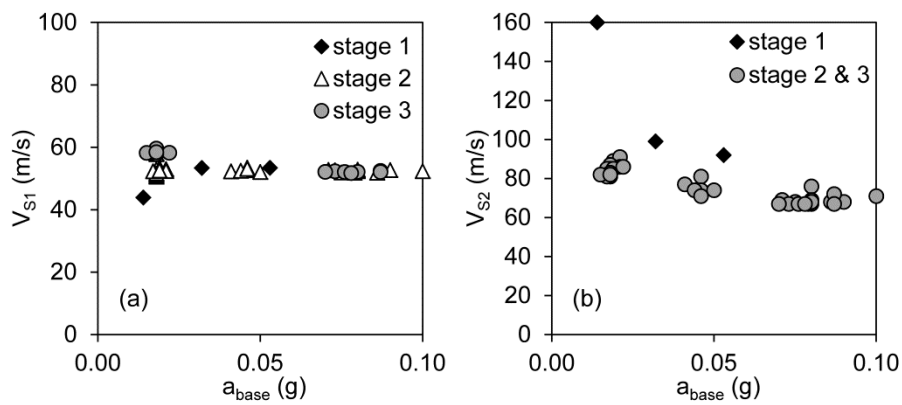


Fig. 10. Shear wave velocity at top layer (a) and bottom layer (b) versus input acceleration level during white noise tests.
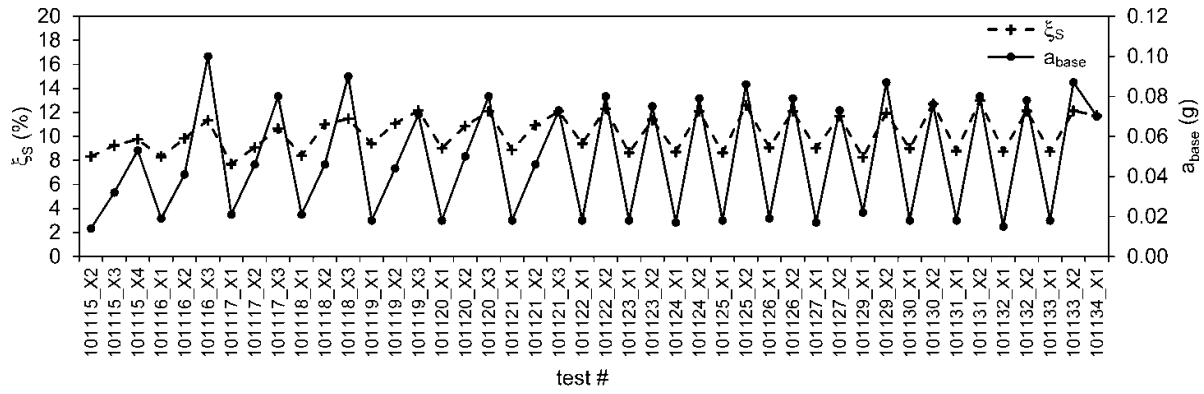
Fig. 11. Variation in damping ratio during white noise tests. Input acceleration level is shown on the right.
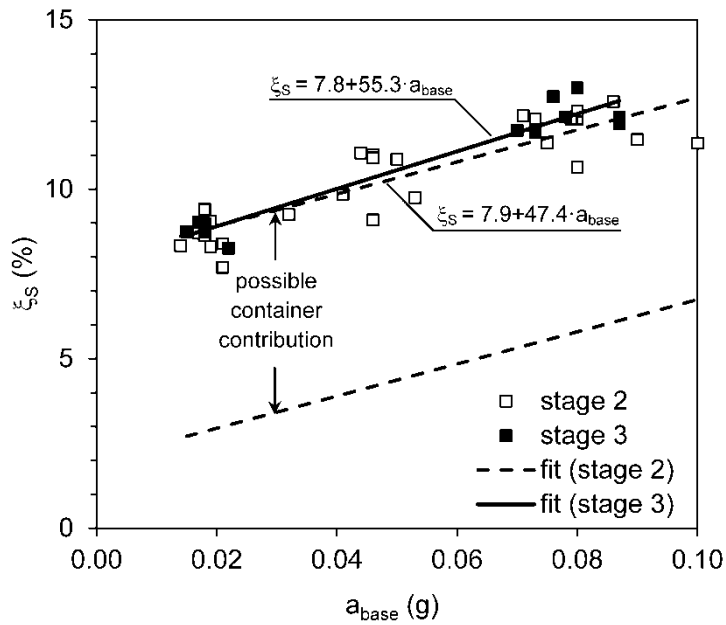


Fig. 12. Damping ratio of soil deposit versus input acceleration level
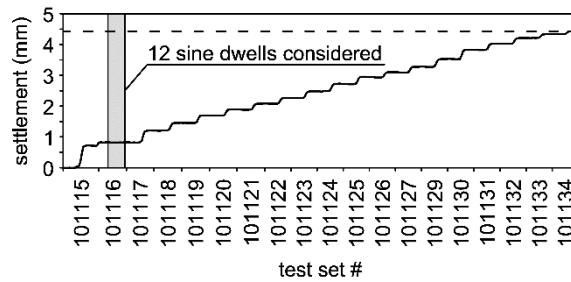


Fig. 13. Cumulative settlement observed during experimental campaign and set of sine dwells considered.

26
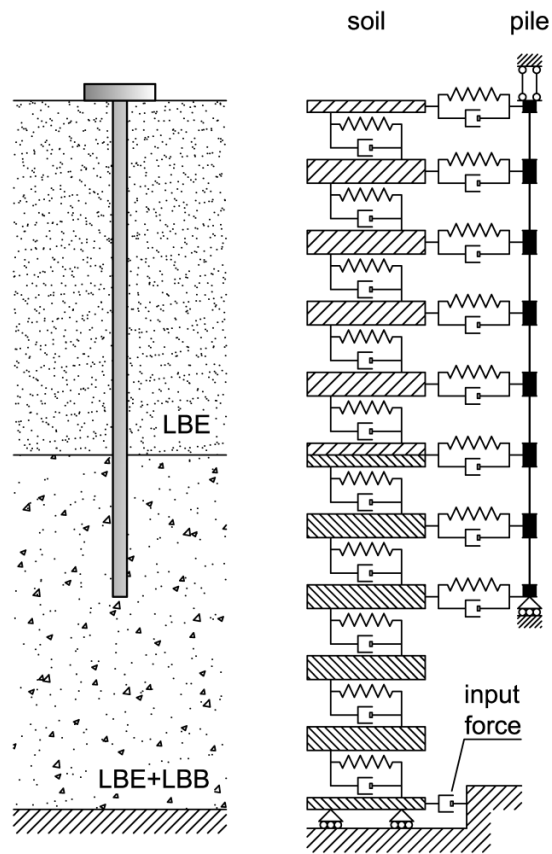
Fig. 14. Nonlinear lumped-parameter model employed for soil and pile.
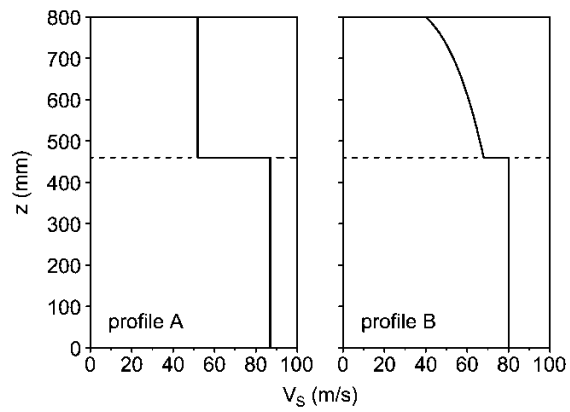


Fig. 15. Shear wave velocity profiles used for modeling the soil deposit
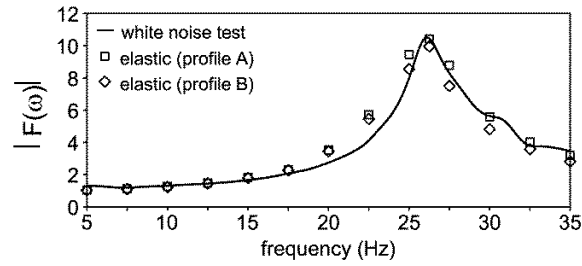
Fig. 16. Calculated linear amplification functions for profiles A and B, and experimental data for white noise test 101116_X1; $a_{base}$=0.02g.
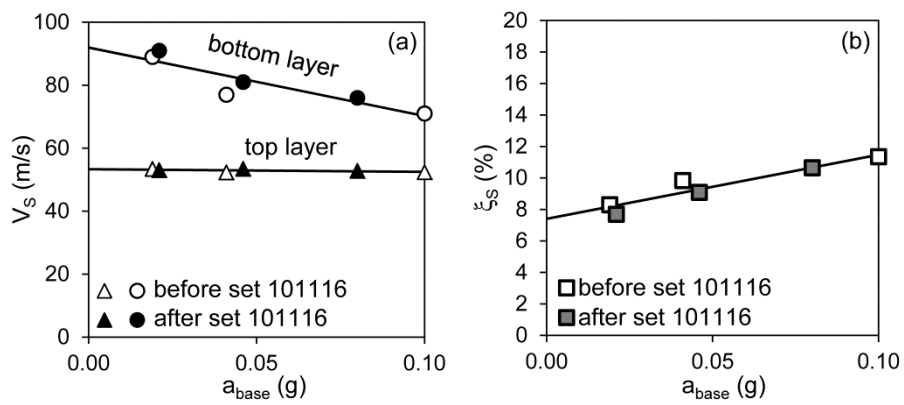


Fig. 17. Variation in shear wave velocity (a) and damping ratio (b) with input acceleration before and after the set of 12 tests considered.
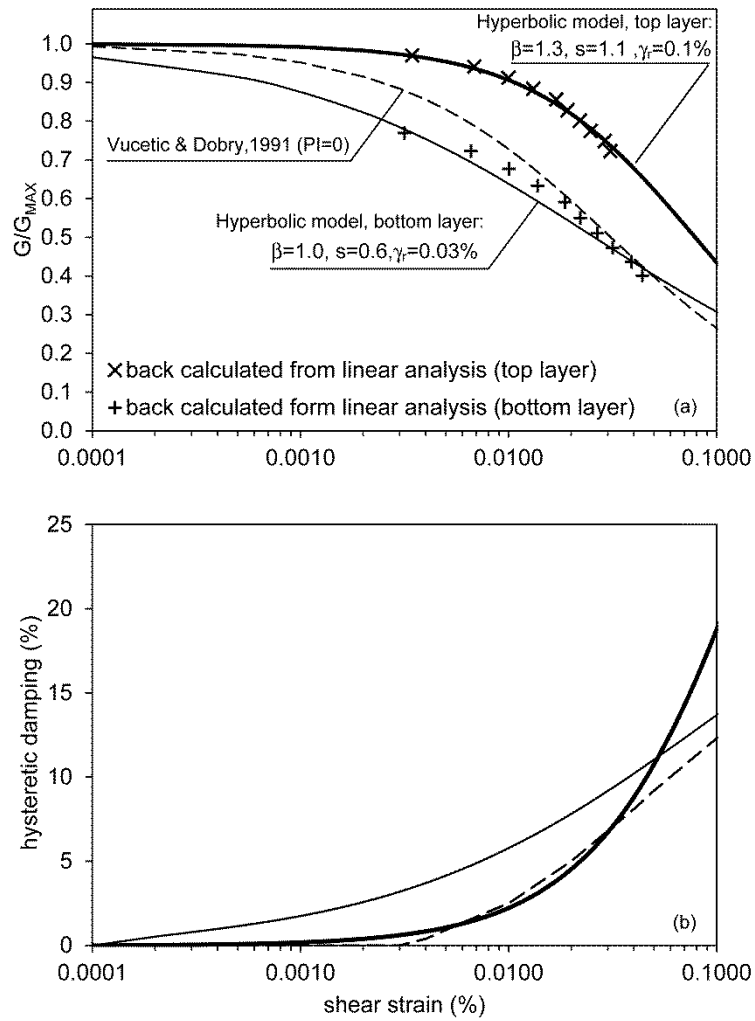
Fig. 18. Back-calculated shear modulus reduction curves (a) and hysteretic damping (b) for the two layers.
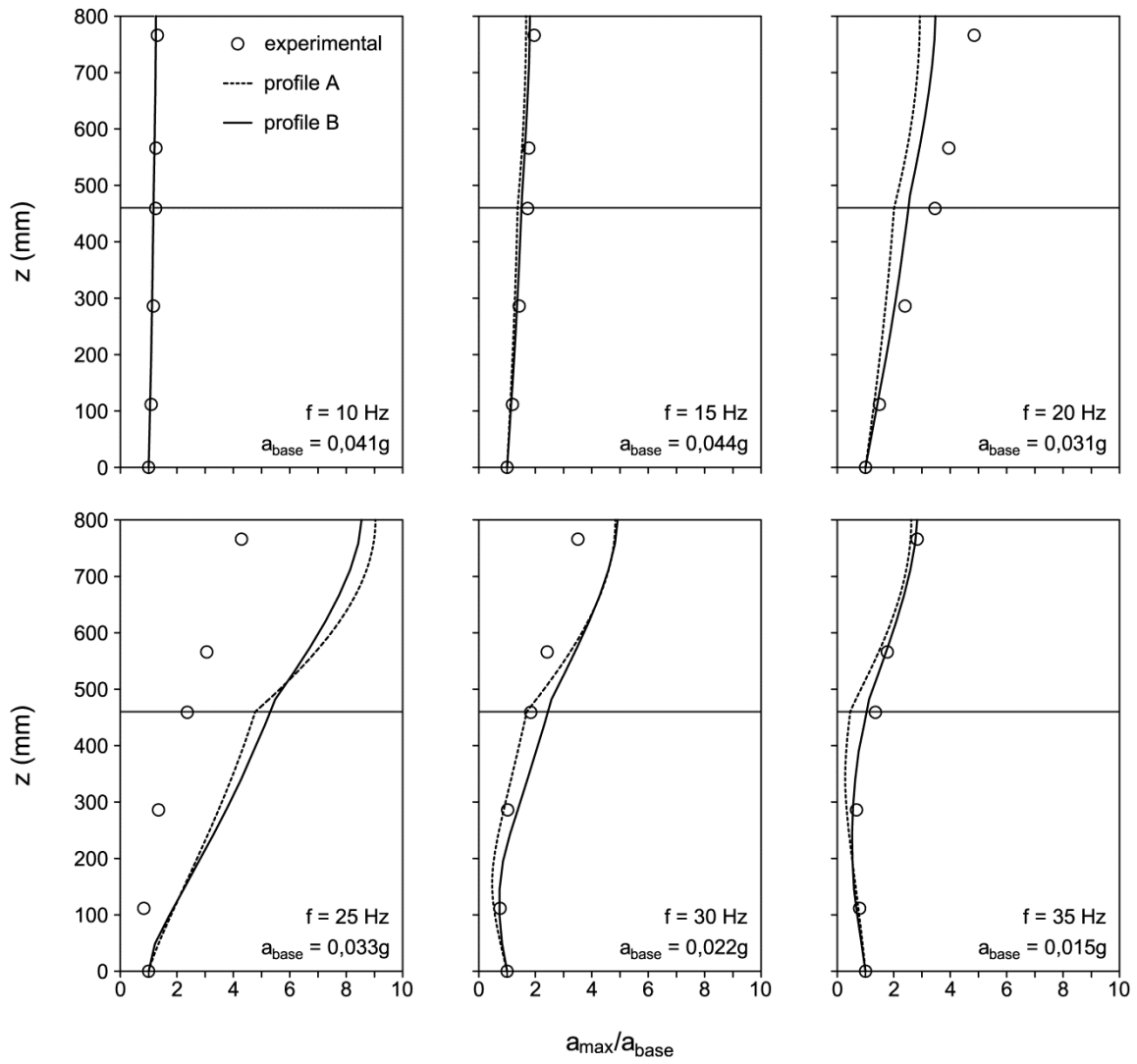
Fig. 19. Maximum acceleration profiles for sine dwell excitation: experimental results versus linear analysis.
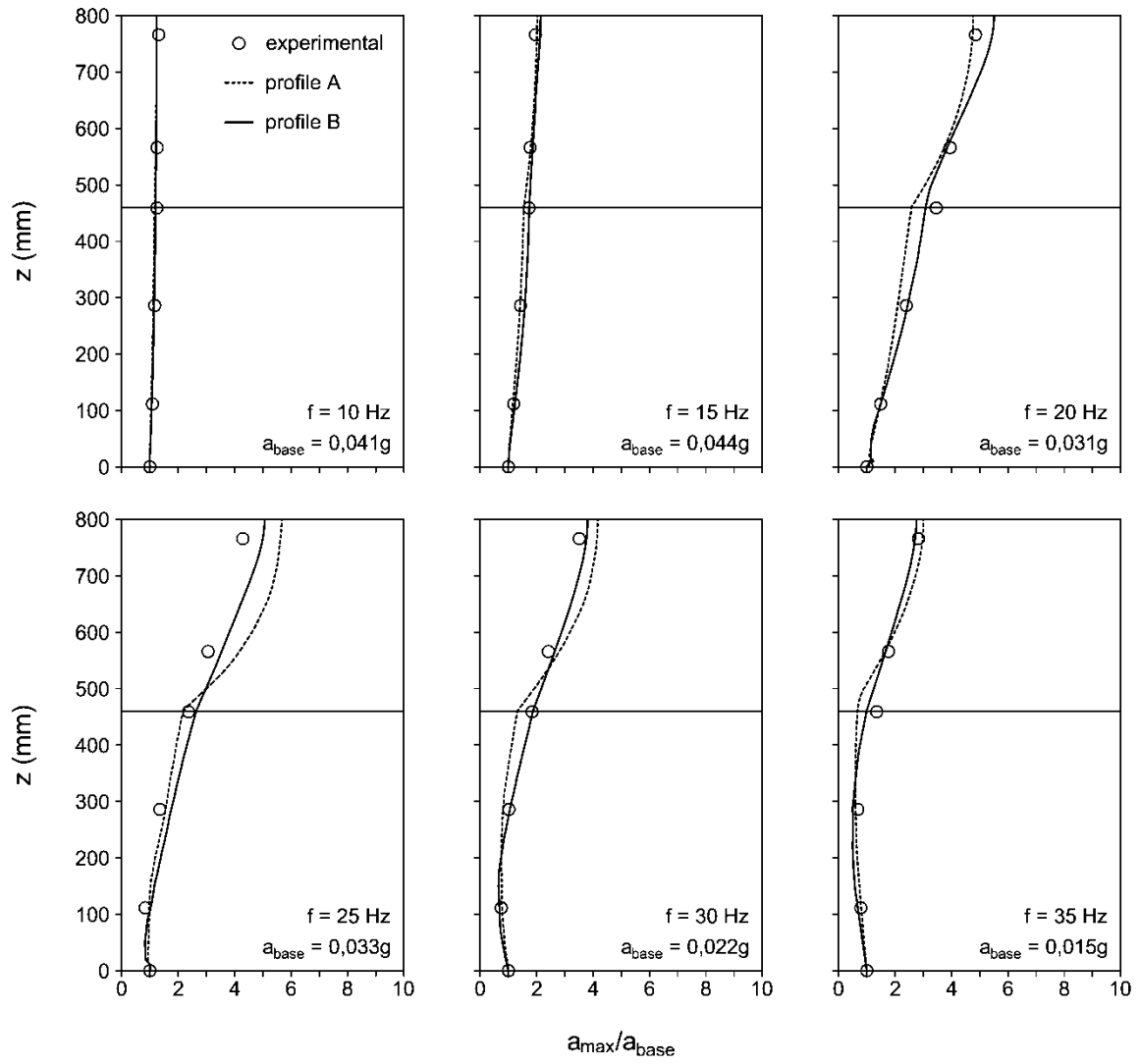
Fig. 20. Maximum acceleration profiles for sine dwell excitation: experimental results versus nonlinear analysis.
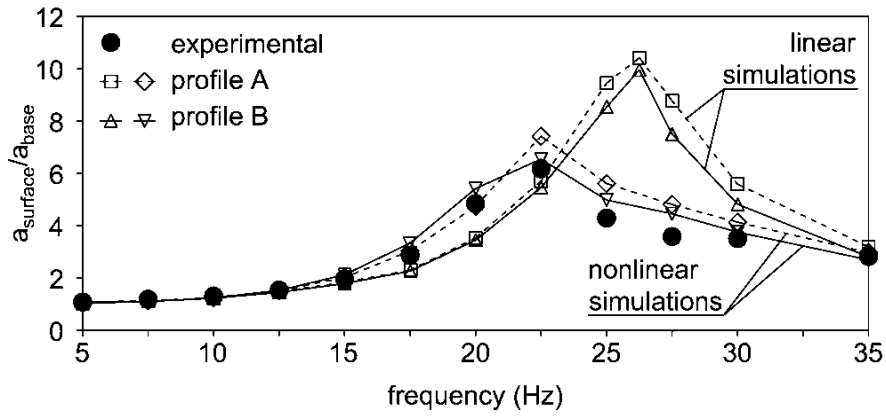
Fig. 21. Effect of soil nonlinearity on free-field surface acceleration for sine dwell excitation of variable frequency; $a_{base} \approx 0.03g$.
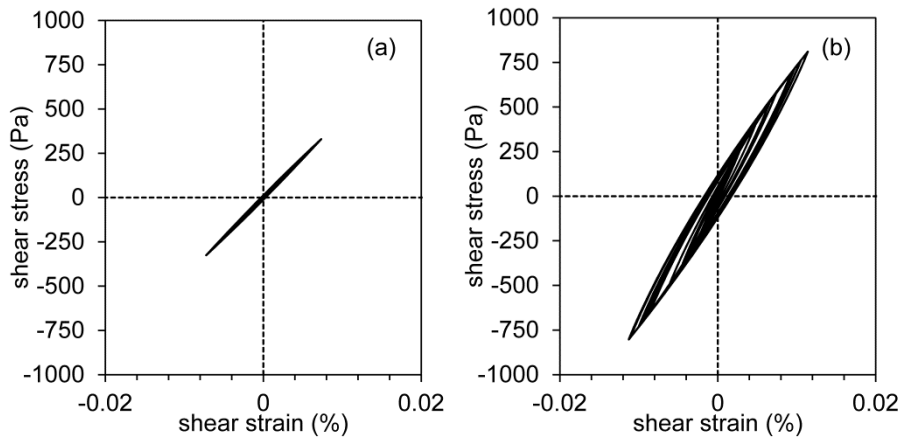


Fig. 22. Hysteretic loops at middle points of upper layer (a) and bottom layer (b) for sine dwell excitation, f=25 Hz, $a_{base} \approx 0.03g$
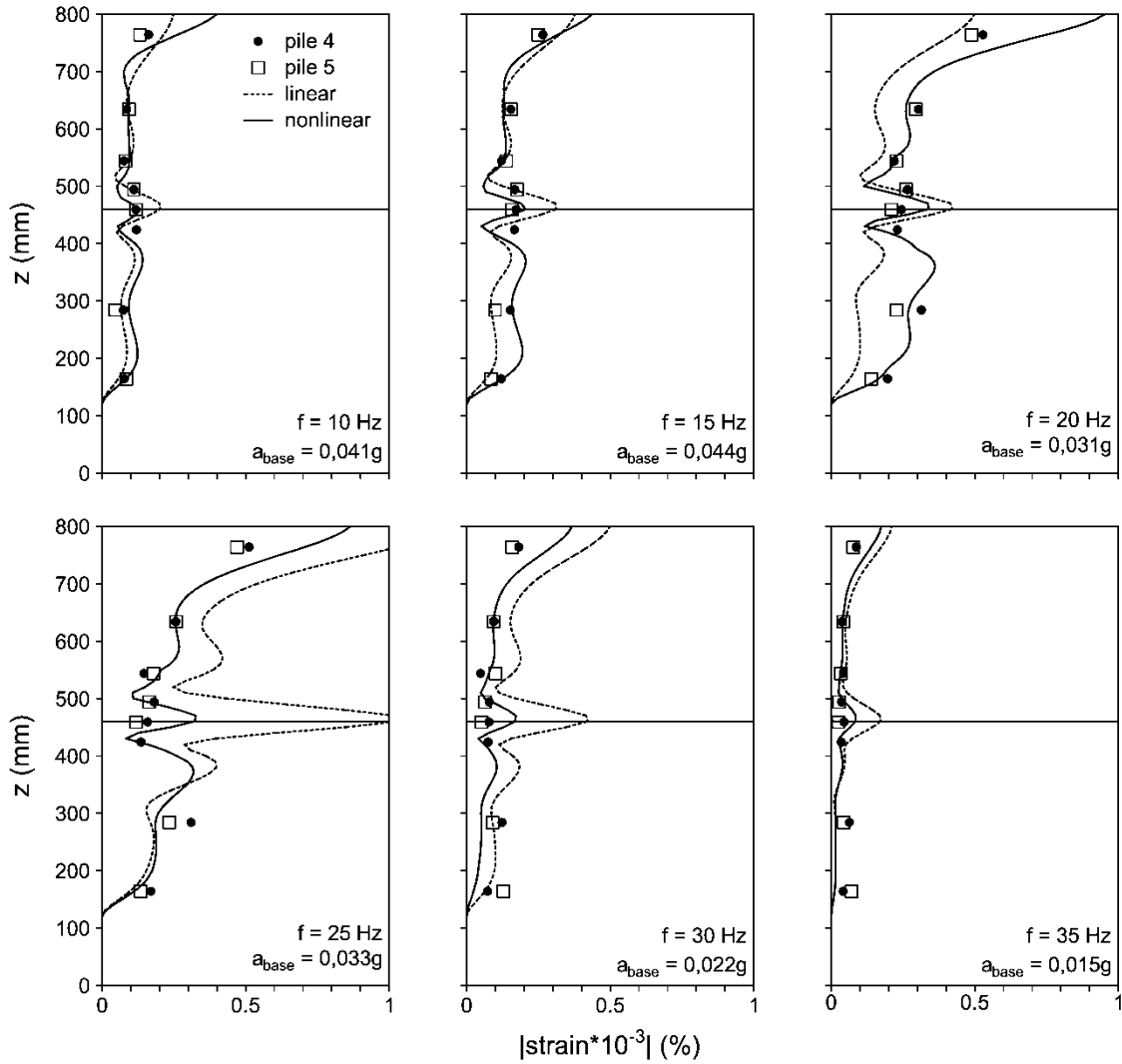
Fig. 23. Maximum bending strains along piles for sine dwell tests: comparisons of experimental measurements and theoretical predictions for soil profile B.
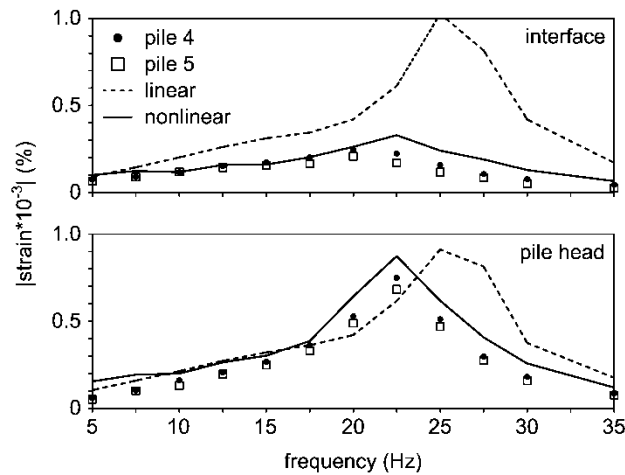


Fig. 24. Maximum bending strains at layer interface and pile head for sine dwell excitations of variable frequency: comparison of experimental measurements and theoretical predictions; $a_{base} \approx 0.03g$.
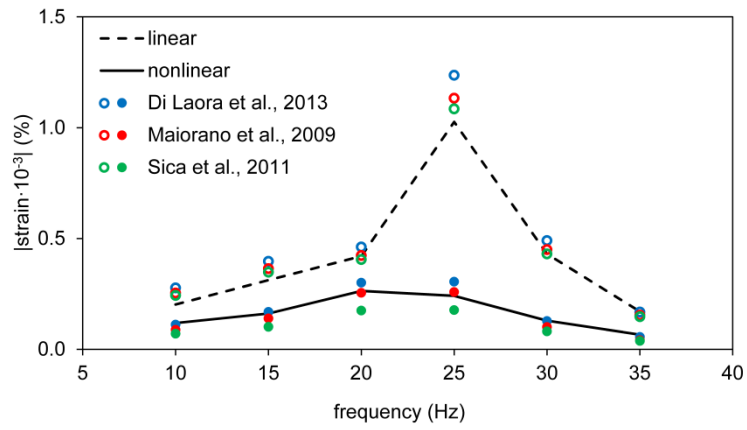
Fig. 25. Kinematic bending strain at the layer interface: comparisons between the present approach and simplified expressions; $a_{base} \approx 0.03g$.

**Table 1**

Leighton Buzzard sands features

| Fraction | Dry density (Mg/m$^3$) | | Grain size diameters (mm) | | | Uniformity coefficient | Source |
|---|---|---|---|---|---|---|---|
| | min | max | $D_{10}$ | $D_{50}$ | $D_{60}$ | $C_u$ | |
| LBE | 1.33 | 1.62 | 0.095 | 0.140 | 0.150 | 1.58 | Cay, 2010 [62] |
| LBB | 1.48 | 1.74 | 0.450 | 0.620 | 0.700 | 1.56 | Visone, 2008 [63] |

**Table 2**

Model pile characteristics

| Parameter | Unit | Value |
|---|---|---|
| Young Modulus | GPa | 70 |
| External Diameter | mm | 22.23 |
| Wall thickness | mm | 0.71 |
| Inertia | mm$^4$ | 2781.7 |
| Bending Stiffness | kNm$^2$ | 0.195 |

**Table 3**

Transducers employed in experiments

| Measured parameter | Transducer type | Description | **Purpose** |
|---|---|---|---|
| Acceleration | Accelerometer Type: SETRA 141A | Total number: 18 High output capacitance type sensor with inbuilt pre-amplifier. Calibrated range: +/-8g. Operating frequency: 0-3000 Hz | Used to measure: Y acceleration of shaking table . Y acceleration of piles head. Y acceleration of free-field. Y acceleration of ESB container. Y acceleration of Oscillator. |
| Strain | Strain gauge Type: EA-13-120LZ-120 (Vishay Ltd) | Total number: 32 Linear strain gauge pattern 3 mm length | Used to measure: Bending strain along piles 4 and 5 shafts . |
| Displacement | Linear Variable Displacement Transformer (LVDTs) Type: RDP DCTH | Total number: 6 | Used to measure: Y displacement of pile head for piles 4 and 5. Rotation of pile head for piles 4 and 5. Y displacement of ESB laminar container. |
| Settlement | Indikon | Total number: 1 | Used to measure: Settlements of the soil surface |

**Table 4**

Considered tests set

| Test type | $a_{base}$ (g) | frequency (Hz) |
|---|---|---|
| Sine dwell | 0.0215 | 5 |
| Sine dwell | 0.0329 | 7.5 |
| Sine dwell | 0.0409 | 10 |
| Sine dwell | 0.0452 | 12.5 |
| Sine dwell | 0.0436 | 15 |
| Sine dwell | 0.0382 | 17.5 |
| Sine dwell | 0.0308 | 20 |
| Sine dwell | 0.0299 | 22.5 |
| Sine dwell | 0.0335 | 25 |
| Sine dwell | 0.0300 | 27.5 |
| Sine dwell | 0.0224 | 30 |
| Sine dwell | 0.0155 | 35 |